

Effect of WO_x on Bifunctional $\text{Pd-WO}_x/\text{Al}_2\text{O}_3$ Catalysts for the Selective Hydrogenolysis of Glucose to 1,2-Propanediol

Chengwei Liu,^{†,§} Chenghua Zhang,^{*,†,‡} Sikai Sun,[‡] Kangkai Liu,[‡] Shunli Hao,[‡] Jian Xu,[‡] Yulei Zhu,^{*,†,‡} and Yongwang Li^{†,‡}

[†]State Key Laboratory of Coal Conversion, Institute of Coal Chemistry, Chinese Academy of Sciences, Taiyuan 030001, People's Republic of China

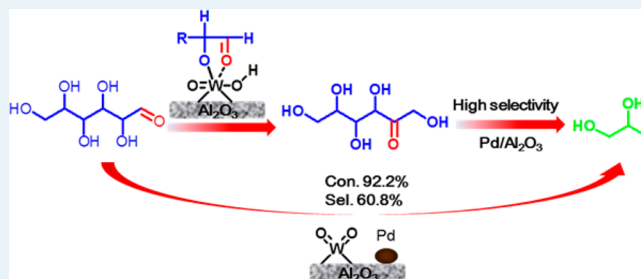
[‡]National Energy Center for Coal to Liquids, Synfuels CHINA Co., Ltd., Huairou District, Beijing, 101400, People's Republic of China

[§]University of Chinese Academy of Sciences, Beijing 100049, People's Republic of China

S Supporting Information

ABSTRACT: A series of $\text{Pd-WO}_x/\text{Al}_2\text{O}_3$ catalysts with different contents of WO_x were prepared by stepwise incipient wetness impregnations. The influence of WO_x on the physicochemical properties of $\text{Pd-WO}_x/\text{Al}_2\text{O}_3$ catalysts, as well as their catalytic performance for the hydrogenolysis of glucose to 1,2-propanediol (1,2-PDO), was investigated. At low surface W density ($0.3\text{--}2.1\text{ W nm}^{-2}$), distorted isolated WO_x and oligomeric WO_x are present on the $\text{Pd-WO}_x/\text{Al}_2\text{O}_3$ catalysts. Furthermore, isolated WO_4 are the dominating species on the $\text{Pd-WO}_x(5\%)/\text{Al}_2\text{O}_3$ catalyst. When the W density increased to 3.1 W nm^{-2} , polymeric WO_x species are dominant on the $\text{Pd-WO}_x(30\%)/\text{Al}_2\text{O}_3$ catalyst. The Pd surface area decreased while the acid amount increased with increasing W density. Furthermore, increased Lewis acid sites are provided by isolated WO_4 and oligomeric WO_x species whereas increased Brønsted acid sites exist on polymeric WO_x species. Lewis acid sites promote glucose isomerization to fructose, which is an intermediate in glucose hydrogenolysis to 1,2-PDO. Metal sites catalyze $\text{C}=\text{O}$ hydrogenation and $\text{C}-\text{C}$ hydrogenolysis, which avoid the coke formation on catalysts. 1,2-PDO selectivity is dependent on the synergy of Lewis acid and metal sites; however, Brønsted acid sites have no contribution to the 1,2-PDO production. Typically, the $\text{Pd-WO}_x(5\%)/\text{Al}_2\text{O}_3$ catalyst possessing the optimal balance of Lewis acid and the metal site shows a 1,2-PDO selectivity of 60.8% at a glucose conversion of 92.2% and has a lifetime of over 200 h.

KEYWORDS: biomass, WO_x , $\text{Pd-WO}_x/\text{Al}_2\text{O}_3$, hydrogenolysis, glucose, 1,2-propanediol, fructose, isomerization



1. INTRODUCTION

Declining fossil fuel reserves, increasing demand for energy, and ongoing global climate change have stimulated intensive interest in developing sustainable resources.^{1,2} In this context, biomass, an inexpensive, renewable, and abundant organic carbon resource, has great potential for use as an alternative feedstock to petroleum in producing liquid fuels and valuable chemicals.^{1,3–5} Accordingly, significant work has been done on the conversion of biomass by various catalytic processes, such as hydrogenolysis,^{6–8} dehydration,^{9,10} oxidation,^{11,12} aqueous-phase reforming,^{13,14} and oligomerization.¹⁵ Among them, one of the most promising processes for biomass transformation is the catalytic hydrogenolysis of biomass to lower polyols. Furthermore, lower polyols, such as 1,2-propanediol (1,2-PDO) and ethylene glycol (EG), are important polyols widely used for pharmaceutical, polyester resins, paints, cosmetics, antifreeze, etc.¹⁶ This process offers a sustainable and economically competitive route for the synthesis of lower

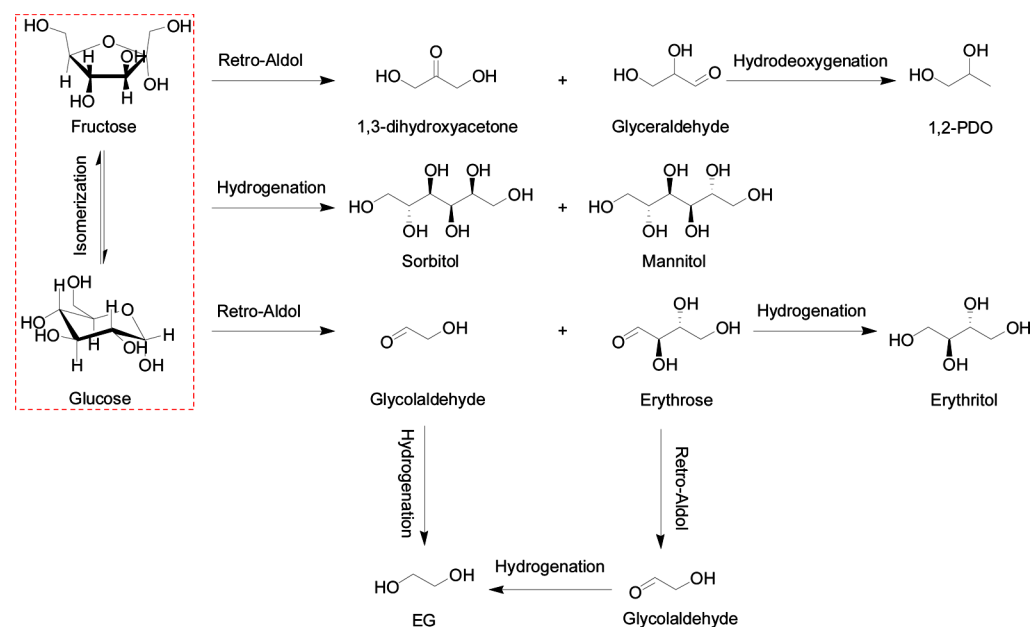
polyols from biomass resources instead of petroleum-based ethylene or propylene oxide.

The hydrogenolysis of sugar and sugar alcohols to lower polyols has been reported since the 1930s. A large number of patents have subsequently appeared.^{17–20} Despite many metallic components and base additives such as $\text{Ca}(\text{OH})_2$ and NaOH being used in the reaction system, the products have contained mainly a mixture of glycerol, 1,2-PDO, and EG. Nowadays, with the abundance of glycerol from biodiesel production, the importance of polyols-related value-added chemicals has shifted toward EG and 1,2-PDO.²¹ Some efforts have been devoted recently to the hydrogenolysis of biomass to 1,2-PDO. Much more recent patents reported by Werpy et al. have described the hydrogenolysis of sugar and sugar alcohol to lower polyols.^{22–24} For example, a supported rhenium-

Received: February 10, 2015

Revised: June 16, 2015

Scheme 1. Possible Reaction Pathway of Glucose Hydrogenolysis



containing multimetallic catalyst was used. The additional metals included Ni, Pd, Ru, Co, Ag, Au, Rh, Ir, Os, and Cu, of which Ni, Pd, and Ru are preferred. Especially, 30% selectivity of 1,2-PDO was obtained in sorbitol hydrogenolysis at 220 °C and 4.14 MPa hydrogen over a Ni–Re/C catalyst. The group of Zhang² has studied the hydrogenolysis of Jerusalem artichoke tuber to 1,2-PDO over Ni–W₂C/AC catalysts and obtained a high yield of 38.5% at 245 °C and 6 MPa H₂. Highly efficient CuCr catalysts have been developed for the conversion of cellulose to 1,2-PDO.⁵ A maximum 1,2-PDO yield of 42.6% at 100% conversion was obtained with Ca(OH)₂ as a cocatalyst. Liu²⁵ obtained 40.9% of PDO yield from cellulose on the Ru/C catalyst combined with 50%WO₃/Al₂O₃ and activated carbon. Apparently, the catalytic process still encountered some challenges, such as environmental problems, poor selectivity, and an unclear reaction mechanism.

Glucose is the most abundant biomass platform molecule in nature and easily soluble in water. Compared with cellulose, glucose is simple in molecular structure, convenient for characterization, and suitable for the study of the catalytic mechanism in catalytic reactions.²⁶ The hydrogenolysis of glucose in aqueous solution can avoid fatal weaknesses in biomass conversion, such as the feedstock transportation, batch reaction, coking, organic solution, environment pollution, etc. All these merits make glucose an ideal feedstock in future large-scale biorefining. However, the aqueous hydrogenolysis of glucose has rarely been studied in recent years. Moreover, highly efficient and stable catalysts are the key factors for the selective conversion of glucose to 1,2-PDO in aqueous solution.

The main reaction pathway of glucose hydrogenolysis to lower polyols has been depicted in the literature.^{25,27–32} As shown in Scheme 1, for glucose hydrogenolysis, hydrogenation, isomerization, retro-aldol condensation, and dehydration reaction occur mainly under hydrothermal and hydrogen atmosphere conditions. It is generally accepted that the hydrogenation of glucose to sorbitol can easily occur under mild conditions over transition metal sites, especially Ni and Ru. The hydrogenation of fructose often produces mannitol. Using several substrates, Wang et al. showed that the retro-aldol

condensation reaction is the dominant pathway for C–C bond cleavage under hydrogenation conditions.³³ The retro-aldol reaction happens mainly at temperatures higher than 160 °C with and without base catalysts.^{34–37} The cleavage of C–O bonds is generally considered to occur via dehydration on acid sites.^{38,39} The hydrogenolysis of glucose to 1,2-PDO under hydrothermal conditions contains two steps: (1) the isomerization of glucose to fructose on Lewis acid/base sites and (2) the retro-aldol condensation reaction of fructose to glyceraldehyde and dihydroxyacetone, followed by dehydration and hydrogenation on metal and acid sites.^{40–42} However, glucose can also undergo retro-aldol condensation to form glycolaldehyde and erythrose, which can be hydrogenated to EG and erythritol, respectively. This reaction route is competitive with glucose isomerization, which is the first step for 1,2-PDO production from glucose. Therefore, a bifunctional catalyst with proper acid and metal sites is required for the isomerization of glucose and the following hydrogenolysis of fructose to 1,2-PDO.

It was reported that supported Pt and Pd catalysts with mineral acids were effective in C–O bond cleavage.^{43,44} Pd has been widely used as the active metal in the selective hydrogenation catalysts.⁴⁵ γ -Al₂O₃ is widely used in industry because of the abundant surface acid sites. Furthermore, γ -Al₂O₃ can promote the isomerization of glucose to fructose.^{46,47} Because of the outstanding catalytic performance, tungsten oxide-based catalysts have been used in many applications, including metathesis and isomerization of alkenes, selective oxidation of unsaturated compounds, selective reduction of nitric oxide, dehydrogenation of alcohols, and hydrodesulfurization and hydrocracking of heavy fractions in the petroleum chemistry. The molecular and electronic structures of the surface WO_x species as well as surface chemical characteristics in supported WO_x catalysts have been extensively investigated.⁴⁸ Moreover, tungsten oxide on alumina was used for hydrotreating and hydrocarbon cracking reactions and emerged as an efficient solid acid catalyst for its changeable acid properties and the strong interaction between WO_x and γ -Al₂O₃.⁴⁹ Therefore, a bifunctional catalyst containing Pd, WO_x,

Table 1. Physicochemical Properties of the Pd–WO_x/Al₂O₃ Catalysts

catalyst	metal loading (mmol g cat. ⁻¹) ^a		W surface density (W nm ⁻²)	<i>d</i> _{PdO} (nm) ^b	<i>d</i> _{Pd} (nm) ^c	<i>d</i> _{Pd} (nm) ^d	chemisorption (μmol CO g cat. ⁻¹) ^d	NH ₃ (μmol g ⁻¹) ^e	Brønsted/ Lewis acid ^f
	Pd	WO _x							
Pd/SiO ₂	0.102					12.9	9.8	0.35	0.0
Pd/Al ₂ O ₃	0.072			4.9		4.2	19.3	53.7	0.0
Pd–WO _x (2%)/Al ₂ O ₃	0.075	0.09	0.3	5.0		4.6	18.1	59.9	0.0
Pd–WO _x (5%)/Al ₂ O ₃	0.072	0.21	0.6	5.5		5.3	15.3	65.0	0.0
Pd–WO _x (10%)/Al ₂ O ₃	0.079	0.41	1.0	6.9		6.9	12.8	73.9	0.0
Pd–WO _x (20%)/Al ₂ O ₃	0.076	0.84	2.1	10.9	11.8	19.0	4.5	77.0	0.06
Pd–WO _x (30%)/Al ₂ O ₃	0.080	1.20	3.1	11.5	13.4	70.1	1.2	84.4	0.51

^aMetal loading determined using ICP. ^bCalculated from Scherrer equation for the peak of PdO (111). ^cThe XRD results of spent catalysts, calculated from Scherrer equation for the peak of PdO (111). ^dCalculated from the CO-pulse chemisorption results. ^eCalculated from the NH₃-TPD results. ^fThe amount of acid sites was determined by quantifying the desorbed pyridine from FT-IR.

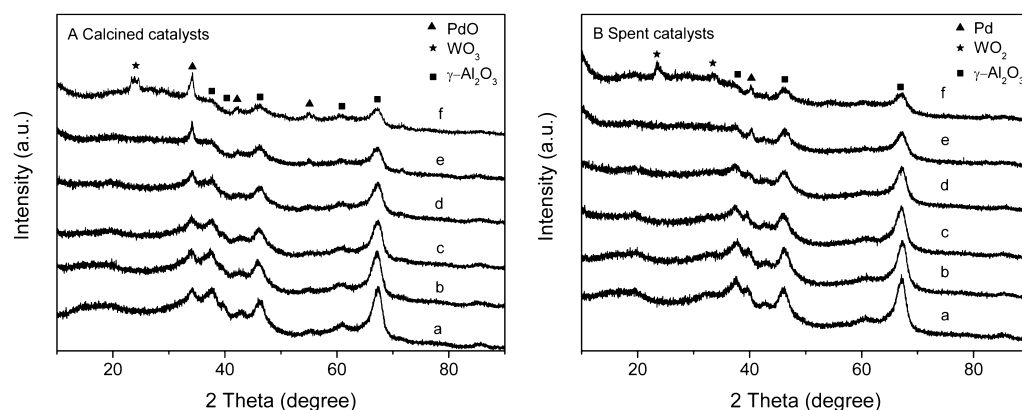


Figure 1. XRD patterns of (A) calcined and (B) spent catalysts: (a) Pd/Al₂O₃, (b) Pd–WO_x(2%)/Al₂O₃, (c) Pd–WO_x(5%)/Al₂O₃, (d) Pd–WO_x(10%)/Al₂O₃, (e) Pd–WO_x(20%)/Al₂O₃, and (f) Pd–WO_x(30%)/Al₂O₃.

and Al₂O₃ components was designed for the hydrogenolysis of glucose to 1,2-PDO.

In this context, a series of bifunctional Pd–WO_x/Al₂O₃ catalysts were first reported for selective hydrogenolysis of glucose to 1,2-PDO. The structure–performance relationship of Pd–WO_x/Al₂O₃ catalysts in glucose hydrogenolysis to 1,2-PDO have been discussed in detail. The role of WO_x in glucose hydrogenolysis to 1,2-PDO was revealed.

2. EXPERIMENTAL SECTION

2.1. Catalyst Preparation. WO_x-modified Pd/Al₂O₃ (denoted as Pd–WO_x/Al₂O₃) catalysts with different WO_x nominal weight loadings in the range of 0–30% were prepared by a stepwise impregnation method. First, the support, γ-Al₂O₃ (purchased from Sinopharm Chemical Reagent Co., Ltd., China), was impregnated with an aqueous solution of (NH₄)₆W₇O₂₄·6H₂O (Sinopharm Chemical Reagent Co., Ltd., China). The impregnated sample was dried overnight at 120 °C and then calcined at 600 °C for 4 h. The obtained sample was then impregnated with an aqueous solution of Pd(NO₃)₂ (Shanxi Kaida Chemical Engineering Co., Ltd.). After impregnation, the sample was dried overnight at 120 °C and then calcined at 500 °C for 4 h. The catalysts were labeled as Pd–WO_x(M)/Al₂O₃, in which M stands for the nominal weight loading of WO_x. The Pd/Al₂O₃ catalyst without WO_x was prepared as the method mentioned above. Prior to the catalytic tests, all the Pd–WO_x/Al₂O₃ and Pd/Al₂O₃ catalysts

were reduced at 500 °C and atmospheric pressure for 1 h with a ramp of 2 °C/min and a hydrogen flow rate of 100 mL/min.

2.2. Catalyst Characterization. The chemical compositions of prepared samples were determined by ICP optical emission spectroscopy (Optima2100DV, PerkinElmer). N₂ physisorption isotherms were measured on a micromeritics ASAP 2420 instrument. Powder X-ray diffraction (XRD) patterns were recorded with a D2/max-RA X-ray diffractometer (Bruker, Germany), operating with Cu Kα radiation at 30 kV and 10 mA. The dispersion and surface area of the palladium were determined by CO pulse chemisorption, which was performed on Auto Chem II 2920 equipment (Micromeritics, USA) with a TCD detector. HRTEM was performed with a Tecnai G2 F30 electron microscope operating at 300 kV. Raman spectra were recorded at room temperature with a LabRAM HR800 system equipped with a CCD detector. The 325 nm of the He–Cd laser was used as the excitation source with a power of 30 MW. UV–vis DRS spectra were collected on an Agilent Cary 5000 UV–vis spectrometer with BaSO₄ as a reference. NH₃ temperature-programmed desorption (NH₃-TPD) measurements were conducted on Auto Chem II 2920 equipment (Micromeritics, USA). The Py-FTIR spectra were obtained using a VERTEX70 Bruker FT-IR spectrometer. X-ray photoelectron spectroscopy (XPS) was recorded on a Thermal XPS ESCALAB 250Xi spectrometer with Al Kα radiation (1486.6 eV) and a multichannel detector. Prior to the test, the calcined sample was reduced in H₂ at 500 °C for 1 h. The obtained binding energies were calibrated using the C 1s peak

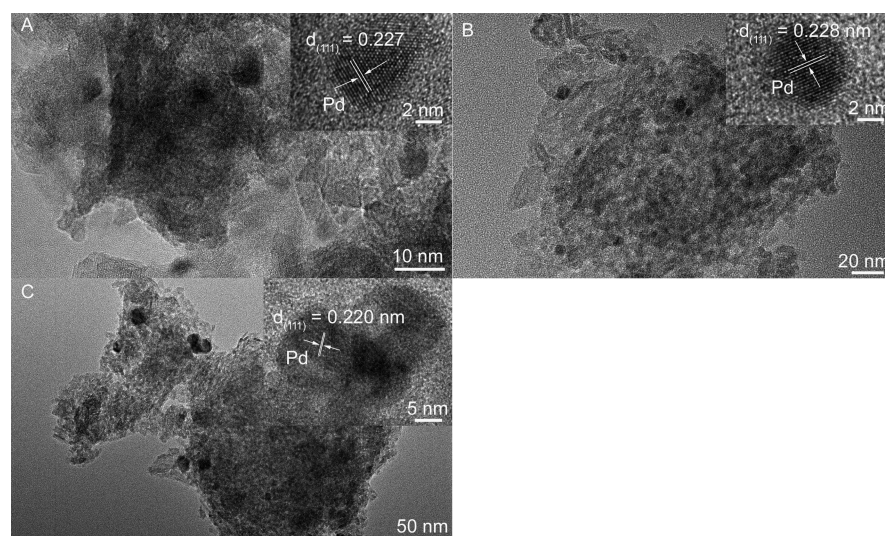


Figure 2. HRTEM images of (A) Pd–WO_x(2%)/Al₂O₃, (B) Pd–WO_x(5%)/Al₂O₃, and (C) Pd–WO_x(20%)/Al₂O₃.

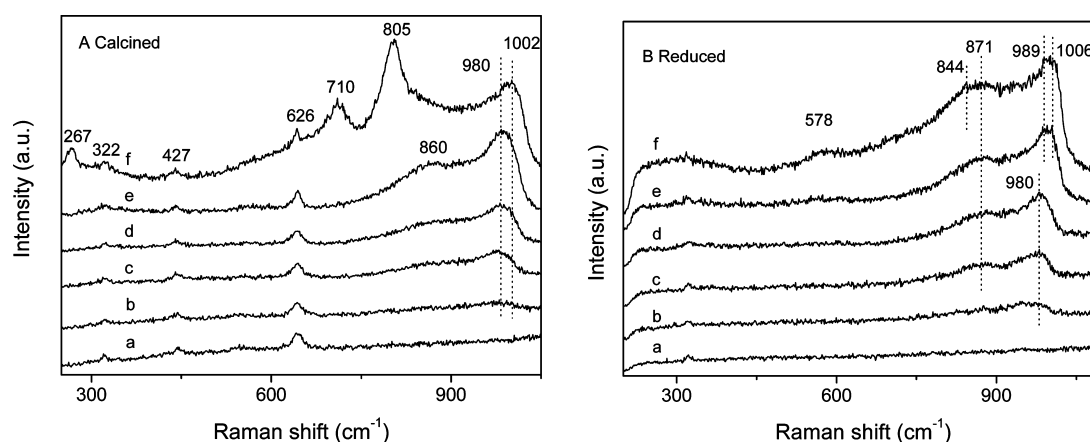


Figure 3. Raman spectra of (A) calcined and (B) reduced catalysts: (a) Pd/Al₂O₃, (b) Pd–WO_x(2%)/Al₂O₃, (c) Pd–WO_x(5%)/Al₂O₃, (d) Pd–WO_x(10%)/Al₂O₃, (e) Pd–WO_x(20%)/Al₂O₃, and (f) Pd–WO_x(30%)/Al₂O₃.

at 284.6 eV as the reference. The experiment error reported in this study is within 0.1 eV. Details are in the [Supporting Information](#).

2.3. Catalytic Reaction Process. The hydrogenolysis of glucose was carried out in a tubular fixed-bed reactor (i.d. 12 mm, length 600 mm) with a cold trap. In a typical run, 2.0 g of catalyst was packed at the isothermal zone and reduced. After reduction, a 5 wt % glucose aqueous solution was introduced into the reactor using a pump along with H₂ cofeeding. The reaction conditions were set as follows: 5 wt % of glucose aqueous solution, 4 MPa H₂ (45 mL/min), 160–220 °C, molar ratio of H₂ to glucose = 22.6:1, WHSV (reactant per gram of catalyst per hour) = 0.48 h^{−1}. The liquid products were collected after 1 h of stable reaction in each temperature point. The total reaction time on-stream was 10 h with temperature increasing from 160 to 220 °C.

3. RESULTS AND DISCUSSION

3.1. Catalyst Characterization. **3.1.1. Structural Properties of Catalysts.** As shown in [Table 1](#), the concentrations of Pd and W were close to the nominal loading as designed, despite a small discrepancy owing to the loss in preparation process. The W surface density determined with ICP-OES and

BET data ([Table S1](#)) varied from 0.3 to 3.1 W nm^{−2} (calculation methods are described in the [Supporting Information](#)).

[Figure 1A](#) displays the XRD patterns of the calcined Pd–WO_x/Al₂O₃ catalysts. All the samples exhibited the characteristic peaks of γ -alumina at $2\theta = 37.4, 46.0,$ and 67.0° .⁵⁰ Obviously, the intensity of the Al₂O₃ characteristic peaks decreased as a result of WO_x loading, reflecting the decrease in the Al₂O₃ molecule coverage on the surface of the catalysts. No diffraction peaks of crystalline WO₃ were observed for Pd–WO_x/Al₂O₃ catalysts with a W density below 3.1 W nm^{−2}, indicating the formation of highly dispersed WO_x species.⁵¹ In addition, the diffraction peaks at $2\theta = 23.3, 23.8,$ and 24.5° were observed on the Pd–WO_x(30%)/Al₂O₃ catalyst, which could be attributed to crystalline phase of WO₃,^{52,53} indicating the agglomeration and low dispersion of tungsten species on the surface of Pd–WO_x(30%)/Al₂O₃. There was also a significant diffraction peak at 33.8° , which is attributed to PdO (JCPDS 75–0584). Furthermore, the intensity of the peak increased obviously with increasing W density to 2.1 and 3.1 W nm^{−2}, indicating the increased PdO crystallite size and the decreased dispersion. The PdO crystallite sizes of the Pd/Al₂O₃, Pd–WO_x(2%)/Al₂O₃, Pd–WO_x(5%)/Al₂O₃, Pd–WO_x(10%)/Al₂O₃, Pd–WO_x(20%)/Al₂O₃, and Pd–WO_x(30%)/Al₂O₃,

estimated from the Scherrer equation, were 4.9, 5.0, 5.5, 6.9, 10.9, and 11.5 nm, respectively.

CO pulse chemisorption was used to determine the Pd dispersion, specific surface area, and particle size. The Pd particle size increased and the dispersion of Pd decreased with increasing W density. CO pulse chemisorption shows that the amount of CO adsorption decreased with increasing W density. The results were consistent with XRD. Compared with XRD results, Pd particle sizes in reduced Pd-WO_x(30%)/Al₂O₃ catalyst were much larger than that in its calcined precursor. It indicates that Pd particles sintered after reduction. To confirm the dispersion and morphology of Pd particles, HRTEM images of reduced samples were obtained (Figure 2). The lattice distances of 0.227, 0.228, and 0.220 nm could be attributed to the (111) planes of face-centered cubic (fcc) Pd (JCPDS 46-1043). It can be observed that the Pd particles with diameters of ~5 nm are uniformly dispersed in the Pd-WO_x(2%)/Al₂O₃ and Pd-WO_x(5%)/Al₂O₃ catalysts; however, large NPs with diameters of ~20 nm are observed on Pd-WO_x(20%)/Al₂O₃, indicating severe agglomeration occurred during reduction. Therefore, the CO pulse chemisorption, XRD, and HRTEM results are in good agreement with each other.

Raman spectroscopy is often used to determine the molecular structures of the bulk and supported tungsten oxide catalysts. Figure 3 shows the Raman spectra of calcined and reduced Pd-WO_x/Al₂O₃ catalysts. The UV excitation was used because of sample fluorescence when excited in the visible region. It is known that the γ -Al₂O₃ support has no Raman resonance. As shown in Figure 3A, the Raman bands at 427 and 626 cm⁻¹ are associated with the Raman-active E_g and B_{1g} vibrational modes of PdO, respectively.⁵⁴ The Raman band around 322 cm⁻¹ originates from a resonance effect induced by the use of laser excitation near the excitation state of PdO.⁵⁴ The broad bands at 980–1002 cm⁻¹ can be ascribed to the symmetric stretching vibration mode of the terminal W=O bonds of well-dispersed tetrahedral WO_x species.^{54–57} The band intensity increases with the increase of the W density. This behavior is indicative of a progressive buildup of WO_x surface species.⁵⁶ Furthermore, the band at 980 cm⁻¹ in the spectra of Pd-WO_x/Al₂O₃ catalysts in the 0.3–2.1 W nm⁻² range is characteristic of highly dispersed WO_x species, such as isolated WO₄ or low-condensed oligomeric (e.g., dipolymer) WO_x species.⁴⁸

A band around 860 cm⁻¹, which can be assigned to the symmetric stretching mode of the W–O–Al,⁴⁸ was also observed. The peak intensity also increased with increasing W density. For Pd-WO_x(30%)/Al₂O₃ catalyst, three new Raman bands at 805, 710, and 267 cm⁻¹ appeared, which could be assigned to W–O stretching, W–O bending, and W–O–W deformation modes of crystalline WO₃ nanoparticles, respectively.⁴⁸ Accordingly, the Raman band shifted from 980 to 1002 cm⁻¹, indicating an increased polymerization of the surface WO_x species.^{49,58} For the reduced samples in Figure 3B, we can see that Raman bands at 980 cm⁻¹ were also observed for the samples in the 0.3–1.0 W nm⁻² range, indicating that the WO_x also presented as tetrahedral coordinated surface species on the reduced samples. However, two bands at 989 and 1006 cm⁻¹ were observed in the spectra of samples in the 2.1–3.1 W nm⁻² range, indicating the present of a mixture of two types of W surface species with different degrees of condensation.⁴⁸ For the reduced Pd-WO_x(30%)/Al₂O₃ catalyst, the Raman bands corresponding to WO₃ disappeared, indicating the reduction of

WO₃ under reduction conditions. The new Raman bands at 844 and 578 cm⁻¹ on Pd-WO_x(30%)/Al₂O₃ reflect the presence of bridging W–O–W bonds, suggesting the higher polymerization of WO_x species.

UV–vis spectra are often used to discriminate between different tungsten oxide species in combination with Raman spectroscopy, such as isolated surface WO_x, oligomeric surface WO_x, and polymeric WO_x (WO₃ NPS or large bulk-like WO₃ particles). The UV–vis spectra of reduced catalysts are shown in Figure 4. A weak band around 271 nm is displayed on the

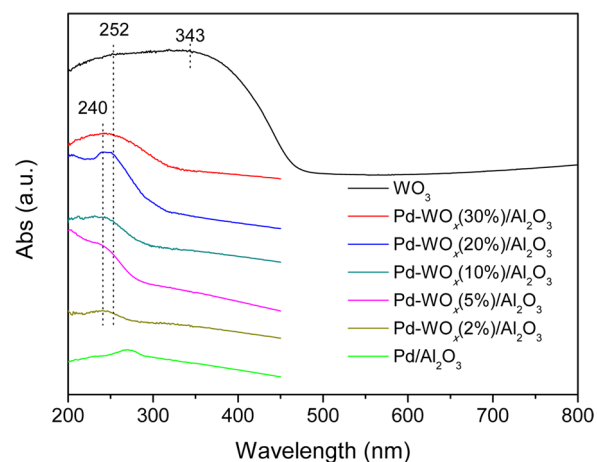


Figure 4. UV–vis DRS spectra of the reduced catalysts.

spectrum of Pd/Al₂O₃. It is negligible compared with the strong absorption of the WO_x species. Crystalline WO₃ is a three-dimensional structure composed of distorted WO₆ units.⁴⁸ Bulk WO₃ contains two ligand-to-metal charge transfer (LMCT) bands at 252 and 343 nm with the corresponding UV–vis DRS E_g value of 2.9 eV (Figure S1 of the Supporting Information).

The UV–vis spectra of Pd-WO_x/Al₂O₃ catalysts are completely different from that of crystalline WO₃, indicating that WO_x species on the Pd-WO_x/Al₂O₃ catalysts are in a highly dispersed form. A band at 240 nm was detected in the spectra of Pd-WO_x/Al₂O₃ catalysts, which could be ascribed to the slightly distorted WO₄ species.⁴⁸ Furthermore, a weak shoulder band at 252 nm was shown in the spectra of Pd-WO_x(20%)/Al₂O₃ and Pd-WO_x(30%)/Al₂O₃ catalysts. However, it is not clear whether the shoulder band exists in the spectra of the catalysts in the 0.3–1.0 W nm⁻² range. As pointed out by Ross-Medgaarden,⁴⁸ several types of tungstate compounds give rise to LMCT band at about 250 nm, such as distorted monotungstate and polytungstates, especially oligomeric unit and polymeric polytungstate species. Therefore, polytungstate species may also exist on the catalysts in the 0.3–1.0 W nm⁻² range. The UV–vis DRS E_g value allows for the discrimination of slightly distorted isolated WO₄/WO₆ (E_g > 4.4 eV) and polymeric structure (E_g < 4.0 eV). Both highly distorted WO₄ and polytungstate species could exist in E_g values of 4.0–4.4 eV. The E_g value for Pd-WO_x(30%)/Al₂O₃ of 3.8 eV is lower than that for other catalysts, reflecting that tungsten species in Pd-WO_x(30%)/Al₂O₃ are polymeric polytungstate. The E_g value for Pd-WO_x(5%)/Al₂O₃ of 4.4 eV is the highest in these catalysts, which is closer to the value of distorted isolated WO₄/WO₆ species. Meanwhile, the shoulder peak at 252 nm was not obvious. It suggests that the WO_x species on the Pd-WO_x(5%)/Al₂O₃ catalyst are present mainly as isolated WO₄. The E_g values for Pd-WO_x(2%)/Al₂O₃, Pd–

$\text{WO}_x(20\%)/\text{Al}_2\text{O}_3$, and $\text{Pd}-\text{WO}_x(10\%)/\text{Al}_2\text{O}_3$ catalysts are 4.0, 4.1, and 4.2 eV, respectively, indicating that tungsten species are present in a mixture of polytungstate and highly distorted isolated WO_4 in these catalysts.

By combining the Raman and UV-vis results, it can be concluded that highly dispersed WO_x species such as highly distorted isolated WO_4 or oligomeric WO_x species are present on the catalyst surface mainly in the $0.3\text{--}2.1\text{ W nm}^{-2}$ range. Especially, the $\text{Pd}-\text{WO}_x(5\%)/\text{Al}_2\text{O}_3$ surface was occupied by isolated WO_4 species. Tungsten species in $\text{Pd}-\text{WO}_x(30\%)/\text{Al}_2\text{O}_3$ are present mainly as polymeric polytungstate.

3.1.2. Acid Properties of the Reduced $\text{Pd}-\text{WO}_x/\text{Al}_2\text{O}_3$ Catalysts. The acid properties of the $\text{Pd}-\text{WO}_x/\text{Al}_2\text{O}_3$ catalysts were measured by NH_3 -TPD and Py-FTIR spectra. NH_3 -TPD profiles and the total acid amount of the reduced samples are shown in Figure S2 and Table 1, respectively. Figure S2A shows that $\text{Pd}-\text{WO}_x/\text{Al}_2\text{O}_3$ catalysts possess broad ammonia desorption curves between 185 and 400 °C, with the central peak at ~ 187 °C, suggesting the presence of main weak acid sites on the sample surface. The acid amounts based on the desorbed NH_3 amounts of these catalysts increase monotonically with increasing surface W density.

The FTIR spectra of adsorbed pyridine were used to study the types of acid sites, as shown in Figure 5. The IR band at

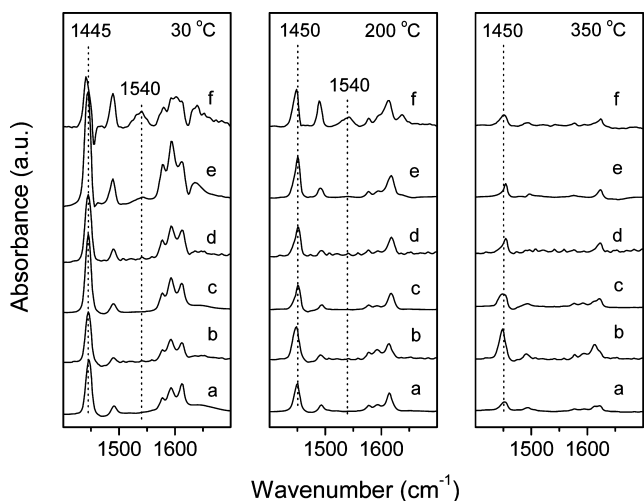


Figure 5. Py-FTIR spectra of the reduced catalysts: (a) $\text{Pd}/\text{Al}_2\text{O}_3$, (b) $\text{Pd}-\text{WO}_x(2\%)/\text{Al}_2\text{O}_3$, (c) $\text{Pd}-\text{WO}_x(5\%)/\text{Al}_2\text{O}_3$, (d) $\text{Pd}-\text{WO}_x(10\%)/\text{Al}_2\text{O}_3$, (e) $\text{Pd}-\text{WO}_x(20\%)/\text{Al}_2\text{O}_3$, and (f) $\text{Pd}-\text{WO}_x(30\%)/\text{Al}_2\text{O}_3$.

1540 cm^{-1} is ascribed to pyridinium ions adsorbed on protonic acid sites, and the band at 1450 cm^{-1} is attributed to pyridine coordinated to Lewis acid sites.⁵⁹ The Lewis acid is present on all the $\text{Pd}-\text{WO}_x/\text{Al}_2\text{O}_3$ catalysts but the protonic acid is present only on catalysts with higher W densities ($2.1\text{--}3.1\text{ W nm}^{-2}$). The intensities of the band at 1450 cm^{-1} decreased significantly as the desorption temperature increased from 30 to 350 °C, indicating the acid sites are mainly composed of weak acid sites. When W density increased to 2.1 W nm^{-2} , a weak band at 1540 cm^{-1} was observed when outgassing at 30 °C and almost disappeared when outgassing at 200 °C, indicating that a small amount of weak Brønsted acid appeared on the catalyst surface. Furthermore, the mole ratio of Brønsted to Lewis acid increased from 0.02 in $\text{Pd}-\text{WO}_x(20\%)/\text{Al}_2\text{O}_3$ to 0.51 in $\text{Pd}-\text{WO}_x(30\%)/\text{Al}_2\text{O}_3$. It suggests that increased Lewis acid sites

are provided mainly by low-condensed polytungstate, especially the isolated WO_4 species, whereas Brønsted acid sites exist mainly on polytungstate, which is consistent with the literature.⁴⁹ Wu reported that the increased Lewis acid sites were related to the coordinatively unsaturated W^{5+} cations, and the Brønsted acid sites arose from partially hydrated tungsten species, including OH groups associated with $\text{W}=\text{O}$, $\text{W}-\text{O}-\text{W}$, and $\text{W}-\text{O}-\text{Al}$ linkages in WO_x clusters.⁵¹

Chen⁵⁰ has studied the correlation between the WO_x structure and the acidity of $\text{WO}_x/\text{Al}_2\text{O}_3$ catalysts. Brønsted acid was negligible for the alumina support and low for a W surface density below 1.4 W nm^{-2} . The amount of Lewis acid decreased, and that of Brønsted acid sites increased with increasing W density in the $1.4\text{--}4\text{ W nm}^{-2}$ range. It was reported that a direct relationship between the amount of Brønsted acid sites and that of the polymeric WO_x surface species exists. A similar relationship was also found on WO_x/ZrO_2 .^{60,61} Moreover, Onfroy⁶⁰ reported that a minimum of the surface W density (above 1.6 W nm^{-2}) of the supported phase was required for the formation of Brønsted acid sites. These results are consistent with the present results in this work.

3.1.3. Surface Chemical States of WO_x Species before and after Reaction. The XPS spectra of W 4f and the deconvoluted ones of the supported WO_x catalysts are shown in Figure 6 and Table 2. As shown in Figure 6A, for the reduced $\text{Pd}-\text{WO}_x(2\%)/\text{Al}_2\text{O}_3$ catalyst, the W 4f doublets at 35.4 and 37.5 eV are attributed to W^{5+} atoms, and peaks at around 37.0 and 39.1 eV are ascribed to W^{6+} atoms.⁶² The molar ratios of $\text{W}^{5+}/\text{W}^{6+}$ on $\text{Pd}-\text{WO}_x/\text{Al}_2\text{O}_3$ catalysts in the $0.3\text{--}0.6\text{ W nm}^{-2}$ range were lower than that in the $1.0\text{--}3.1\text{ W nm}^{-2}$ range, indicating that WO_x in the higher W density is easily reduced. After reaction, the ratios of $\text{W}^{5+}/\text{W}^{6+}$ of the $\text{Pd}-\text{WO}_x(2\%)/\text{Al}_2\text{O}_3$ and $\text{Pd}-\text{WO}_x(5\%)/\text{Al}_2\text{O}_3$ catalysts did not change. It suggests that the valence state of the highly isolated tungsten species was stable during the reaction. However, the ratios of $\text{W}^{5+}/\text{W}^{6+}$ of $\text{Pd}-\text{WO}_x(10\%)/\text{Al}_2\text{O}_3$, $\text{Pd}-\text{WO}_x(20\%)/\text{Al}_2\text{O}_3$ and $\text{Pd}-\text{WO}_x(30\%)/\text{Al}_2\text{O}_3$ decreased obviously after reaction, indicating that the reduced polymeric tungsten species are susceptible to oxidation in steam atmosphere during the glucose hydrogenolysis.

3.2. Catalytic Performance of $\text{Pd}-\text{WO}_x/\text{Al}_2\text{O}_3$ in Glucose Hydrogenolysis. The activity and selectivity of the $\text{Pd}-\text{WO}_x/\text{Al}_2\text{O}_3$ catalysts for glucose hydrogenolysis are shown in Figure 7 and Table 3. For the product distribution, only a trace amount of CH_4 was detected in the gas phase, with the yield below 0.2%. No CO or other gas products were detected. Except for the large amount of isomerization and hydrogenation products of C_6 species that were fructose and sorbitol in liquid phase, a wide variety of hydrogenolysis products, including ethanol, EG, glycerol, 1,2-PDO, isopropyl alcohol, propanol, erythritol, 1,2-butanediol (1,2-BDO), 2-butanol, xylitol, 1,2-pentanediol, and 1,2-hexanediol, were detected.

Table 3 shows that the selectivities of EG and 1,2-BDO changed slightly with the loading of WO_x species. Glucose can undergo retro-aldol condensation to form glycolaldehyde and erythrose, which can be hydrogenated to EG and erythritol, respectively. Furthermore, erythrose can also undergo further dehydration and hydrogenation reaction to form 1,2-BDO. The results suggest that WO_x species have nearly no effect on the retro-aldol condensation of glucose or the dehydration of the intermediates. Furthermore, fructose and 1,2-PDO were the predominant products. However, only fructose was the main product in the liquid phase on $\text{WO}_x(5\%)/\text{Al}_2\text{O}_3$, with the

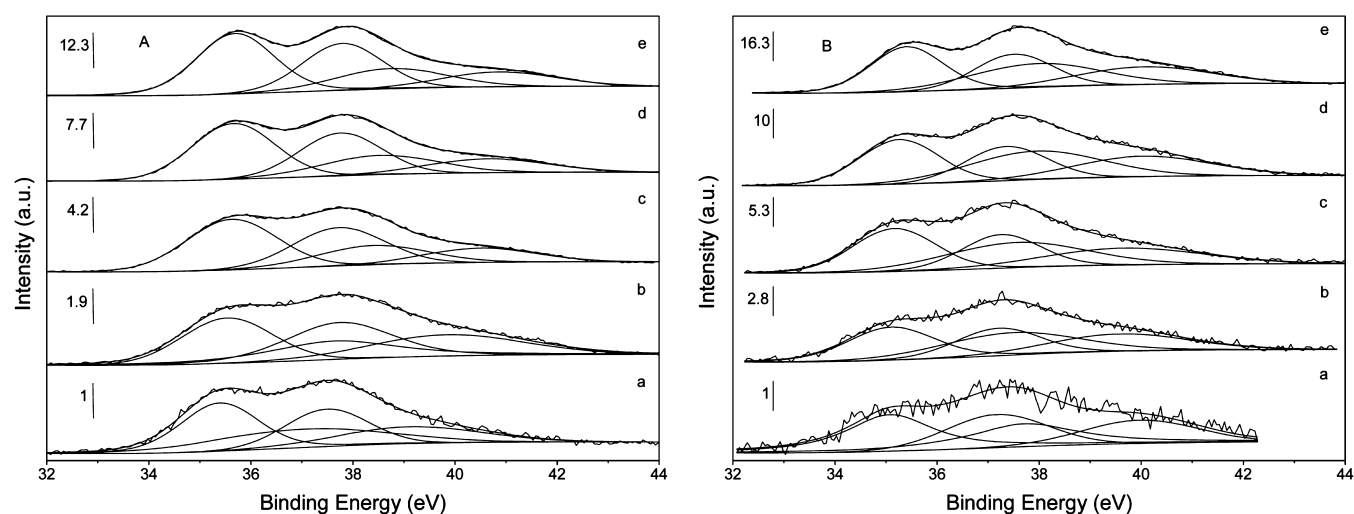


Figure 6. W 4f XPS spectra of the (A) reduced and (B) spent catalysts: (a) Pd–WO_x(2%)/Al₂O₃, (b) Pd–WO_x(5%)/Al₂O₃, (c) Pd–WO_x(10%)/Al₂O₃, (d) Pd–WO_x(20%)/Al₂O₃, and (e) Pd–WO_x(30%)/Al₂O₃.

Table 2. XPS Parameters of the W 4f Region in Pd–WO_x/Al₂O₃ Samples

sample	binding energy for W 4f (eV) ^a				W ⁵⁺ /W ⁶⁺	
	W ⁶⁺ W 4f _{5/2}	W ⁶⁺ W 4f _{7/2}	W ⁵⁺ W 4f _{5/2}	W ⁵⁺ W 4f _{7/2}	after reduced	after reaction
Pd–WO _x (2%)/Al ₂ O ₃	39.1 (39.8)	37.0 (37.7)	37.5 (37.2)	35.4 (35.1)	1.3	1.3
Pd–WO _x (5%)/Al ₂ O ₃	39.8 (39.6)	37.7 (37.5)	37.6 (37.2)	35.5 (35.1)	0.9	1.0
Pd–WO _x (10%)/Al ₂ O ₃	40.5 (39.7)	38.4 (37.6)	37.7 (37.3)	35.6 (35.2)	2.2	1.0
Pd–WO _x (20%)/Al ₂ O ₃	40.6 (40.0)	38.5 (37.9)	37.8 (37.4)	35.7 (35.3)	2.1	1.0
Pd–WO _x (30%)/Al ₂ O ₃	40.9 (40.1)	38.8 (38.0)	37.8 (37.5)	35.7 (35.4)	2.2	1.1

^aThe B.E. values outside parentheses are ascribed to W_{4f} of the reduced Pd–WO_x/Al₂O₃ catalysts. The B.E. values in parentheses are assigned to W_{4f} of the spent Pd–WO_x/Al₂O₃ catalysts.

selectivity of 67.9% at 160 °C. Furthermore, the fructose selectivity decreased to 24.1% when the temperature increased to 180 °C, with most of the feedstock cooking in the reactor. It is known that glycerol and 1,2-PDO easily undergo further degradation under an acid environment.⁶³ In this work, except for glycerol and 1,2-PDO, only a trace amount of propanol with a selectivity lower than 1% was detected; however, no other C₃ products, such as propanal, propylene, or propane, were detected. The results show that 1,2-PDO showed very low hydrogenolysis activity under this condition, which must be related to the reaction conditions and catalyst properties. The carbon balance, in the percentage of carbon accounted (both in liquid and gas phase), decreased with increasing temperature. It suggests that glucose was coked at a higher temperatures. Furthermore, the carbon balance was above 85% for all Pd–WO_x/Al₂O₃ catalysts at 160 and 180 °C.

Figure 7A shows that the activity of glucose hydrogenolysis increased with the increase in the temperature. The selectivity of fructose decreased sharply with increasing temperature; however, the selectivity of 1,2-PDO increased first and then decreased with an increase in the temperature. It displayed that 180 °C was an optimal temperature for 1,2-PDO production. The doping of WO_x influences not only the catalytic activity but also the product selectivity. The conversion of glucose increased first and then decreased with increasing W density at 180 °C. For the product selectivity shown in Figure 7B, fructose selectivity decreased first and then increased with increasing W density at 180 °C. The selectivity of 1,2-PDO showed a trend completely the opposite of fructose, as shown in Figure 7C. 1,2-PDO selectivity increased first and then

decreased with increasing W density. The maximum selectivity was obtained on Pd–WO_x(5%)/Al₂O₃ at 180 °C, with the highest value being 60.8%, which is one of the best performances reported in this reaction.

3.3. The Property-Performance Relationship of Pd–WO_x/Al₂O₃ Catalysts in Glucose Hydrogenolysis to 1,2-PDO. H₂ pressure plays an important role in glucose hydrogenolysis. In the pressure range of 2.0–7.5 MPa, hydrogenation is considered to be the first-order kinetics of hydrogen pressure.⁶⁴ Furthermore, lowering the hydrogen pressure is expected to decrease the activity of glucose hydrogenation to sorbitol, increase the activity of retro-aldol reaction, and improve the selectivity to lower polyols.^{41,65} Ooms reported that when the hydrogen pressure was lowered from 60 to 45 bar, the sorbitol yield decreased and the ethylene glycol yield slightly increased. However, a further decrease in hydrogen pressure to 30 bar resulted in a lower ethylene glycol yield and an unfavorable carbon mass balance. To inhibit the hydrogenation of glucose to sorbitol and improve the carbon mass balance, 4 MPa was applied for glucose hydrogenolysis.

Usually, a small metal size or large specific area means a high hydrogenation capability; however, the glucose conversions do not strictly follow the monotonic decreasing tendency of Pd specific area in these Pd–WO_x/Al₂O₃ catalysts, proving that Pd is not the sole influencing factor in glucose conversion. Unfortunately, the variation of acidity does not coincide with the tendency of activities and 1,2-PDO selectivities of catalysts. Combined with the 1,2-PDO selectivity, metal surface area, and acid amount, we can see that 1,2-PDO was dependent on the synergy of the metal and acid sites, and an excellent catalytic

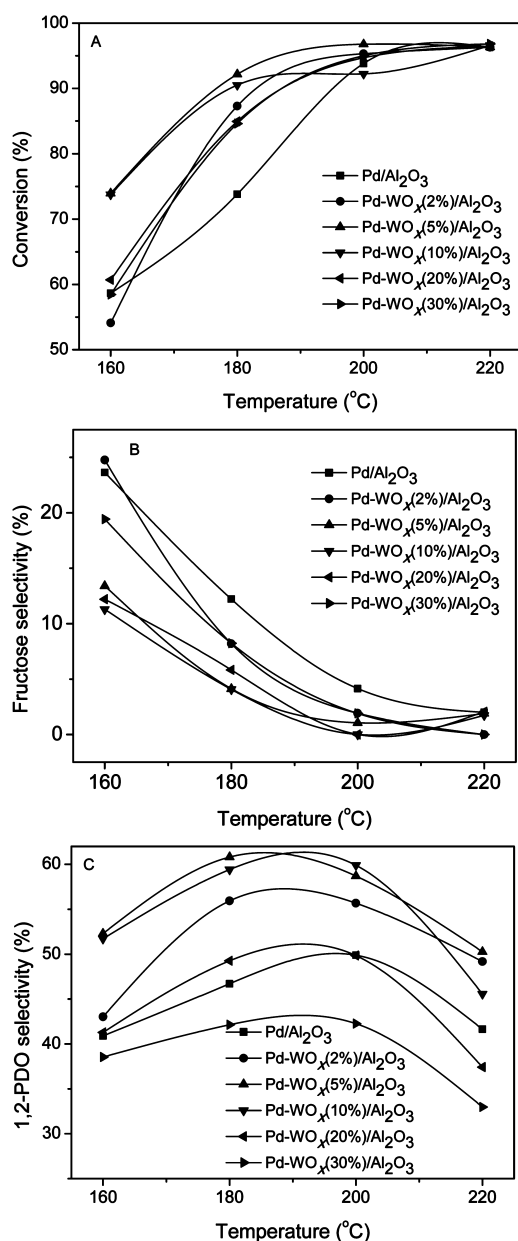


Figure 7. Glucose conversion and product distribution on Pd-WO_x/Al₂O₃ catalysts: (A) glucose conversion, (B) fructose selectivity, (C) 1,2-PDO selectivity. Reaction conditions: 4 MPa H₂, 5 wt % glucose aqueous solution, molar ratio of H₂ to glucose = 22.6:1, WHSV = 0.48 h⁻¹.

performance was reached on Pd-WO_x(5%)/Al₂O₃. To reveal the mechanism of the synergy of metal and acid sites, their individual roles in the reaction route should be investigated.

A Pd/SiO₂ catalyst with nearly no acidity was designed to study the effect of metal sites on glucose conversion and 1,2-PDO selectivity (Figure S2B and Table S2 of the Supporting Information and Table 1; a lower reduction temperature of 200 °C was used for the catalytic tests and characterization to inhibit the sintering of Pd particles). The results showed that Pd/SiO₂ had very poor activity for the conversion of glucose, with values of 3.6 and 19.6% at 160 and 180 °C, respectively. Furthermore, sorbitol was the main product with the selectivity of 74.6% and 57.4% at 160 and 180 °C, respectively. In contrast, 1,2-PDO selectivity was only 11.0 and 16.1%. The

results show that the Pd metal sites on this acid-free catalyst surface mainly act as a hydrogenation function but have quite low C–C bond cleavage capability.

To understand the intrinsic function of the acid site in the reaction, model reactions of glucose hydrogenolysis on Al₂O₃ and WO_x(5%)/Al₂O₃ in H₂ and N₂ atmosphere were investigated (Table S3 of the Supporting Information). The results indicate that the pure acid catalysts show an isomerization selectivity of glucose to fructose but quite low hydrogenation activity. However, a large amount of humins was observed on both catalysts. Furthermore, the exact humin products are too complicated to be identified, which inhibits us from understanding the role of acid sites in glucose conversion. When the 1,2-PDO selectivity and the characterization results of acidity are combined, it can be found that the increased Lewis acid on the Pd-WO_x/Al₂O₃ catalysts with lower W densities (0–1.0 W nm⁻²) could promote glucose hydrogenolysis to 1,2-PDO and the increased Brønsted acid has no additional contribution to 1,2-PDO selectivity. This phenomenon indicates that a Lewis acid plays important roles in catalyzing glucose to 1,2-PDO. Therefore, it is worthwhile to study the exact role of these structures that result in the Lewis acid in glucose hydrogenolysis.

3.4. Effect of the Structure of WO_x on Glucose Hydrogenolysis to 1,2-PDO. As indicated by the above results, the Pd-WO_x(5%)/Al₂O₃ catalyst shows excellent selectivity to 1,2-PDO. Meanwhile, the W species in this catalyst are present as isolated WO₄. It indicates that the isolated WO₄ species plays the vital role in the 1,2-PDO production.

The ratios of W⁵⁺/W⁶⁺ of the Pd-WO_x/Al₂O₃ after reaction were nearly the same, especially in the 0.6–3.1 W nm⁻² range. However, these catalysts showed obvious difference on glucose conversion and 1,2-PDO selectivity. It suggests that the catalytic performances were independent of the valence state of tungsten. To further reveal the function of the WO_x structure in glucose conversion, the hydrogenolysis of glucose on bulk WO₃ crystal and Pd/WO₃ was conducted; the results are shown in Table 4. WO₃ showed nearly no activity for glucose conversion. Furthermore, both WO₃ and Pd/WO₃ showed very low selectivity for 1,2-PDO. It suggests that the crystalline WO₃ or highly polymerized WO_x species have no contribution to the hydrogenolysis of glucose and 1,2-PDO production. Indeed, the highly dispersed WO_x species, especially the isolated WO₄ species, promote glucose conversion and improve the 1,2-PDO selectivity. However, it is unclear how these structures catalyze the reaction. It is worth studying and discussing them in depth.

3.5. The Mechanism of the Promoting Effect of WO_x for Glucose Hydrogenolysis to 1,2-PDO. To study the mechanism of glucose hydrogenolysis to 1,2-PDO on Pd-WO_x/Al₂O₃, the hydrogenolysis of fructose on Pd/Al₂O₃ and Pd-WO_x(5%)/Al₂O₃ catalysts was performed; the results are shown in Table 5. It is shown that fructose hydrogenolysis showed higher conversion and higher 1,2-PDO selectivity than glucose hydrogenolysis on Pd/Al₂O₃ catalyst (as shown in Table 5). It indicates that glucose hydrogenolysis is a cascade reaction. This reaction contains at least two consecutive reactions: glucose isomerization to fructose and fructose hydrogenolysis to 1,2-PDO. Moreover, glucose isomerization is a rate-determining step for glucose conversion. Sasaki⁴¹ has conducted retro-aldol condensation of glucose in supercritical water. They pointed out that retro-aldol condensation was a key reaction for saccharide degradation in high-temperature

Table 3. Activity and Selectivity of Pd–WO_x/Al₂O₃ Catalysts for Glucose Hydrogenolysis at 160 and 180 °C^a

sample	T (°C)	conv (%)	selectivity (%)								
			sor	fru	gly	EG	1,2-PDO	1,2-BDO	CH ₄	others ^b	carbon balance
WO _x (5%)/Al ₂ O ₃	160	26.7	0.0	67.9	5.3	0.9	6.5	0.0	0.0	19.4	99.5
	180	67.6	0.0	24.1	1.5	0.9	6.4	1.3	0.0	65.8	41.7
Pd/Al ₂ O ₃	160	58.6	6.8	23.6	9.1	4.0	40.9	4.2	0.2	11.2	99.5
	180	73.8	3.6	12.2	8.8	5.1	46.7	6.7	0.2	16.7	95.3
Pd–WO _x (2%)/Al ₂ O ₃	160	54.1	7.3	24.8	9.8	3.7	43.0	4.3	0.2	6.9	99.2
	180	87.3	2.4	8.2	7.3	4.0	55.9	8.1	0.2	13.9	93.7
Pd–WO _x (5%)/Al ₂ O ₃	160	74.0	6.1	13.4	8.8	5.2	52.3	5.9	0.2	8.1	99.4
	180	92.2	2.3	4.1	7.2	5.7	60.8	9.9	0.1	9.9	97.8
Pd–WO _x (10%)/Al ₂ O ₃	160	73.7	5.7	11.3	8.1	4.7	51.7	7.1	0.2	11.2	99.6
	180	90.5	2.2	4.1	6.6	5.2	59.4	10.9	0.1	11.5	98.6
Pd–WO _x (20%)/Al ₂ O ₃	160	60.7	4.0	12.2	7.9	6.1	41.3	6.9	0.2	21.4	95.3
	180	84.9	2.0	5.8	6.5	5.5	49.3	10.7	0.2	20.0	94.8
Pd–WO _x (30%)/Al ₂ O ₃	160	58.4	0.0	19.4	9.4	5.8	38.6	7.0	0.2	19.6	95.5
	180	84.6	0.0	8.2	6.1	4.6	42.1	9.9	0.2	28.9	85.7

^aReaction conditions: 4 MPa H₂, 5 wt % glucose aqueous solution, molar ratio of H₂ to glucose = 22.6:1, WHSV = 0.48 h⁻¹. ^bOthers: ethanol, EG, isopropyl alcohol, propanol, erythritol, 2-butanol, xylitol, 1,2-pentanediol, and 1,2-hexanediol, etc. sor = sorbitol, fru = fructose, gly = glycerol.

Table 4. Glucose Conversion over Model Catalysts^a

catalyst	atmosphere	conv. (%)	yield (%)							
			fru	ery	EG	gly	1,2-PDO	1,2-BDO	2-butanol	others
blank	H ₂	0.0	0.0	0.0	0.0	0.0	0.0	0.0	0.0	0.0
WO ₃	H ₂	3.7	0.0	0.0	0.0	0.0	2.5	0.5	0.2	0.5
Pd/WO ₃	H ₂	16.1	0.0	0.0	1.2	1.4	3.9	1.1	0.2	8.3

^aReaction conditions: 4 MPa H₂, 180 °C, 5 wt % glucose aqueous solution, molar ratio of H₂ to glucose = 22.6:1, WHSV = 0.48 h⁻¹. fru = fructose, ery = erythritol, gly = glycerol.

Table 5. Activity and Selectivity of Pd–WO_x/Al₂O₃ Catalysts for Fructose Hydrogenolysis at 160 and 180 °C^a

sample	T (°C)	conv (%)	selectivity (%)							
			glu	sor	ery	EG	gly	1,2-PDO	1,2-BDO	others ^b
Al ₂ O ₃	180	68.8	15.2	0.0	3.7	0.5	0.9	5.9	0.0	73.8
WO _x (5%)/Al ₂ O ₃	180	80.3	8.7	0.0	2.5	1.4	2.3	6.8	0.0	78.3
Pd/Al ₂ O ₃	160	78.8	4.7	7.6	5.8	5.8	10.9	52.6	4.3	8.3
	180	95.0	3.9	2.9	3.7	8.1	9.3	57.0	6.8	8.3
Pd–WO _x (5%)/Al ₂ O ₃	160	88.3	8.2	5.8	6.2	5.0	8.8	56.8	5.0	4.2
	180	97.7	2.7	2.0	3.0	4.5	6.5	62.2	7.7	11.4

^aReaction conditions: 4 MPa H₂, 5 wt % fructose aqueous solution, molar ratio of H₂ to fructose = 22.6:1, WHSV = 0.48 h⁻¹. ^bOthers: ethanol, EG, isopropyl alcohol, propanol, 2-butanol, xylitol, 1,2-pentanediol, and 1,2-hexanediol, humins, etc. glu = glucose, sor = sorbitol, ery = erythritol, gly = glycerol.

water. Glycolaldehyde and erythrose, intermediates of C₂ and C₄ polyol, could be obtained from retro-aldol condensation of glucose in supercritical water, whereas glyceraldehyde and dihydroxyacetone, intermediates of C₃ polyols, could be obtained from retro-aldol condensation of fructose. The isomerization of glucose to fructose also occurred in supercritical water. Furthermore, they also proposed that fructose was the intermediate for the conversion of glucose to C₃ products (glyceraldehyde and dihydroxyacetone). Kanie⁴² found that fructose hydrogenolysis displayed higher 1,2-PDO selectivity than glucose hydrogenolysis on Pt nanoparticles. Isomerization between glucose and fructose proceeded at a temperatures as low as 403 K and could be accelerated by Pt nanoparticles and H₂. They suggested that the isomerization of glucose to fructose was the intermediate reaction step for the hydrogenolysis of glucose to 1,2-PDO.

Comparing Pd/Al₂O₃ and Pd–WO_x(5%)/Al₂O₃, the activity and 1,2-PDO selectivity are largely improved by WO_x addition

when glucose is the feedstock (as shown in Table 3); however, they are only slightly increased by WO_x when fructose is the feedstock (as shown in Table 5). It suggests that the tungsten addition improves the isomerization of glucose to fructose, but it has no obvious effect on the hydrogenolysis of fructose to 1,2-PDO. These results indicate that fructose is highly active and acts as the key intermediate for the production of 1,2-PDO. Combined with all these results, it can be concluded that the exact role of the dispersed WO_x in glucose hydrogenolysis to 1,2-PDO is catalyzing the isomerization step from glucose to fructose and having a slightly promoting effect on the selective conversion of fructose to 1,2-PDO. As we have known, the highly dispersed WO_x or isolated WO₄ species provide the Lewis acid sites in catalysts; therefore, it is proposed that the Lewis acid-related structures could also catalyze the isomerization of glucose to fructose. This speculation is also supported by the model reaction on Al₂O₃ for glucose hydrogenolysis, which shows a fructose selectivity of 42.7% (as shown in Table

S2). Davis et al.⁶⁶ and Choudhary⁶⁷ have reported that the isomerization reaction can be promoted by a Lewis acid in the catalyst. The Lewis acid could polarize the carbonyl group in the ketone, which follows an intramolecular hydride shift mechanism between the carbonyl-containing C-1 and the hydroxyl-bearing C-2 of glucose.

As shown in Scheme 2A, isolated tetrahedral WO_4 species provide the Lewis acid sites. The structure of isolated WO_4

Scheme 2. Probable Structures of (A) Isolated WO_4 or (B) Tetrahedral AlO_4 Species on $\text{Pd-WO}_x/\text{Al}_2\text{O}_3$



species has also been proposed by many researchers.^{48,68} It is well-known that the $\gamma\text{-Al}_2\text{O}_3$ surface is composed of mainly octahedral and tetrahedral Al sites.^{69,70} Furthermore, it is suggested experimentally and theoretically that a tetrahedral surface Al site has a stronger Lewis acidity than an octahedral one.^{69,70} The tetrahedral AlO_4 structure on $\gamma\text{-Al}_2\text{O}_3$ surface is shown in Scheme 2B. In addition, Davis et al.⁶⁶ found that Sn incorporated in the framework of zeolite Beta, which is also present as tetrahedral coordination and acts as Lewis acid, performed the isomerization reaction following an intramolecular hydride shift mechanism between the carbonyl-containing C-1 and hydroxyl-bearing C-2 of glucose by a way of a 5-member complex. Therefore, a similar promoting mechanism of WO_4 or AlO_4 is proposed in Scheme 3, considering the isomerization on Lewis acid sites provided by isolated WO_4 or tetrahedral AlO_4 species. Furthermore, the conversions of fructose on Al_2O_3 and $\text{WO}_x(5\%)/\text{Al}_2\text{O}_3$ were also studied to distinguish the roles of acid sites provided by WO_x species and alumina, which is shown in Table 5. The results showed that fructose conversion was higher on $\text{WO}_x(5\%)/\text{Al}_2\text{O}_3$ than that on Al_2O_3 . It suggests that WO_x species could promote fructose conversion. However, $\text{WO}_x(5\%)/\text{Al}_2\text{O}_3$ showed lower glucose selectivity than Al_2O_3 . It indicates that WO_x species could promote the isomerization of glucose to fructose and inhibit the reverse reaction. Compared with Al_2O_3 , both of them can promote the isomerization of glucose to fructose. In this respect, we suppose

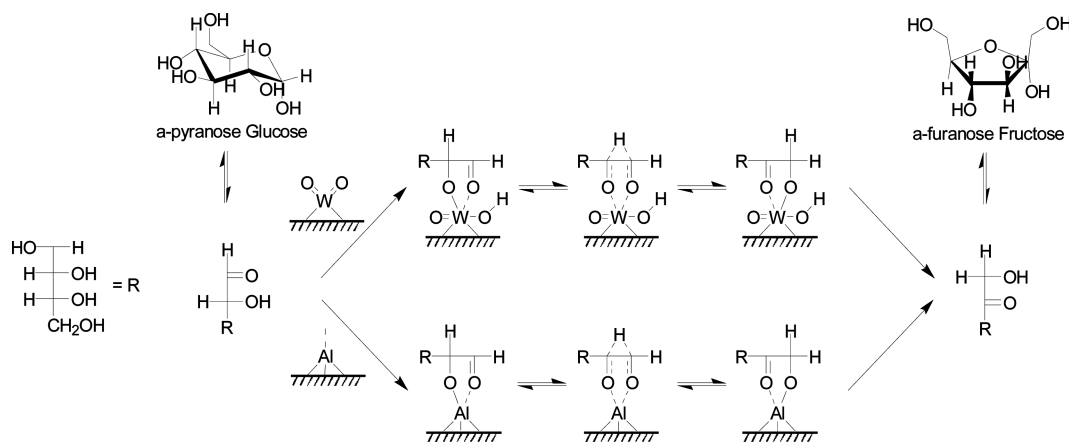
that they play similar roles and run in parallel in the hydrogenolysis of glucose. Moreover, WO_x species could also inhibit the reverse conversion of glucose isomerization to fructose and promote the conversion of fructose to lower polyols, which makes it an efficient component in catalysts for glucose hydrogenolysis to 1,2-PDO.

3.6. The Stability of $\text{Pd-WO}_x/\text{Al}_2\text{O}_3$ Catalyst in Glucose Hydrogenolysis to 1,2-PDO. To investigate the stability of the catalysts, their structural properties after reaction were also studied by ICP, BET, CO pulse chemisorption, and XRD (Table 1, Figure 1, and Table S3). The BET, ICP, and CO pulse chemisorption results of $\text{Pd-WO}_x(5\%)/\text{Al}_2\text{O}_3$ are nearly the same before and after reaction, which indicates that structure damage, leaching, and sintering of the active sites were negligible. From Figure 1 we can see the XRD patterns of Al_2O_3 were nearly the same as that of the calcined samples. It suggested that Al_2O_3 was stable in the hydrothermal condition during the reaction. The diffraction peak of PdO disappeared, whereas the peak at 40.0° was detected for all the spent catalysts that could be ascribed to Pd^0 (JCPDS 46-1043). However, the Pd peaks were not clear enough for the calculation of the Pd particle size. The peak intensity of Pd in the $2.1\text{--}3.1\text{ W nm}^{-2}$ range was also higher than that in the lower W density. The estimated Pd particle sizes in Table 1 are 11.8 and 13.4 nm for $\text{Pd-WO}_x(20\%)/\text{Al}_2\text{O}_3$ and $\text{Pd-WO}_x(30\%)/\text{Al}_2\text{O}_3$, respectively, which are slightly higher than that of the PdO in the calcined samples. The stability of the $\text{Pd-WO}_x(5\%)/\text{Al}_2\text{O}_3$ catalyst was also tested at different WHSVs (Figure 8). The activities and selectivities remained stable over 200 h. It turned out that $\text{Pd-WO}_x(5\%)/\text{Al}_2\text{O}_3$ had good stability. Metal leaching into the liquid phase after 12 h on-stream was detected. The results showed that no leaching of Pd was detected, and only a trace amount of W, 1.48 mg/L, was detected in the liquid phase. The results confirmed the stability of the catalyst.

CONCLUSION

An efficient and stable $\text{Pd-WO}_x/\text{Al}_2\text{O}_3$ catalyst was designed for the selective hydrogenolysis of glucose to 1,2-PDO. Highly dispersed WO_x species, such as distorted isolated WO_4 and oligomeric WO_x species, are present in the $0.3\text{--}2.1\text{ W nm}^{-2}$ range, and polymeric WO_x species are present mainly on the $\text{Pd-WO}_x(30\%)/\text{Al}_2\text{O}_3$ catalyst. Furthermore, distorted isolated

Scheme 3. Mechanism of Promoting Effect of Isolated WO_4 or AlO_4 Species on $\text{Pd-WO}_x/\text{Al}_2\text{O}_3$ for the Isomerization of Glucose to Fructose



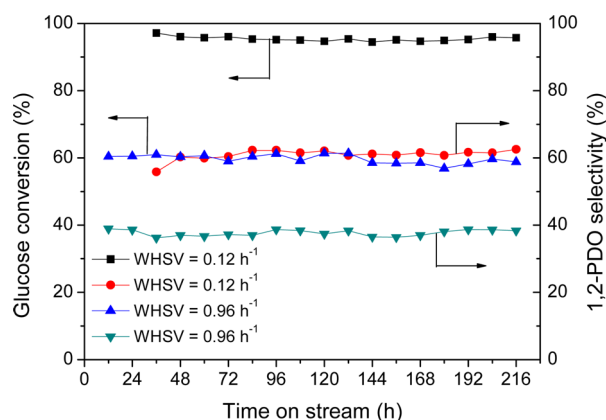


Figure 8. Stability of the Pd-WO_x(5%)/Al₂O₃ catalyst in the hydrogenolysis of glucose at different values of WHSV. Reaction conditions: 180 °C, 4 MPa H₂, 5 wt % glucose aqueous solution, molar ratio of H₂ to glucose = 22.6:1.

WO₄ species are present mainly on the Pd-WO_x(5%)/Al₂O₃ catalyst. Only Lewis acid sites are present in the 0.3–1.0 W nm⁻² range provided by the alumina support and highly dispersed WO_x species. Brønsted acid sites also appear in the 2.1–3.1 W nm⁻² range provided by polytungstate species. Both the Lewis acid sites and Pd metal sites are active sites for glucose hydrogenolysis to 1,2-PDO. The hydrogenolysis of glucose to 1,2-PDO is strongly dependent on the synergy of the Lewis acid sites and Pd metal sites. Pd metal catalyzes the hydrogenation of C=O in glucose and intermediates and has weak C–C bond cleavage capability. Lewis acids can promote the isomerization of glucose to fructose and show a slight promoting effect on the selective conversion of fructose to 1,2-PDO. Fructose is the key intermediate for highly selective production of 1,2-PDO. Lewis acid is provided by highly dispersed WO_x species, such as isolated WO₄ and oligomeric WO_x species, and by tetrahedrally coordinated AlO₄ species. Furthermore, highly distorted isolated WO₄ species showed excellent promoting effect for the hydrogenolysis of glucose to 1,2-PDO. By the promotion of WO_x, Pd-WO_x(5%)/Al₂O₃ showed a 60.8% of 1,2-PDO selectivity at glucose conversion of 92.2%. The catalyst also showed good stability, with a lifetime of more than 200 h.

ASSOCIATED CONTENT

Supporting Information

The Supporting Information is available free of charge on the ACS Publications website at DOI: 10.1021/acscatal.5b00800.

Details of catalyst preparation and product analysis methods; UV–vis DRS spectra and E_g values of the Pd-WO_x/Al₂O₃ catalysts and WO₃ (Figure S1); NH₃-TPD patterns of the reduced catalysts and Py-FTIR pattern of reduced Pd/SiO₂ (Figure S2); The BET surface area of the Pd-WO_x/Al₂O₃ catalysts (Tables S1); glucose conversion over different model catalysts and in different atmospheres (Table S2); comparison of the structure properties of Pd-WO_x(5%)/Al₂O₃ before and after reaction (Table S3) (PDF)

AUTHOR INFORMATION

Corresponding Authors

*E-mail: zhangchh@sxicc.ac.cn.

*E-mail: zhuyulei@sxicc.ac.cn.

Notes

The authors declare no competing financial interest.

ACKNOWLEDGMENTS

This work was financially supported by the Major State Basic Research Development Program of China (973 Program) (No. 2012CB215305).

REFERENCES

- Jiménez-Morales, I.; Moreno-Recio, M.; Santamaría-González, J.; Maireles-Torres, P.; Jiménez-López, A. *Appl. Catal., B* **2015**, *164*, 70–76.
- Zhou, L.; Wang, A.; Li, C.; Zheng, M.; Zhang, T. *ChemSusChem* **2012**, *5*, 932–938.
- Sun, R.; Wang, T.; Zheng, M.; Deng, W.; Pang, J.; Wang, A.; Wang, X.; Zhang, T. *ACS Catal.* **2015**, *5*, 874–883.
- Huang, Z.; Chen, J.; Jia, Y.; Liu, H.; Xia, C.; Liu, H. *Appl. Catal., B* **2014**, *147*, 377–386.
- Xiao, Z.; Jin, S.; Pang, M.; Liang, C. *Green Chem.* **2013**, *15*, 891–895.
- Fabičovicová, K.; Malter, O.; Lucas, M.; Claus, P. *Green Chem.* **2014**, *16*, 3580–3588.
- Grilc, M.; Veryasov, G.; Likozar, B.; Jesih, A.; Levec, J. *Appl. Catal., B* **2015**, *163*, 467–477.
- Zhang, J.; Teo, J.; Chen, X.; Asakura, H.; Tanaka, T.; Teramura, K.; Yan, N. *ACS Catal.* **2014**, *4*, 1574–1583.
- Dabbawala, A. A.; Mishra, D. K.; Huber, G. W.; Hwang, J.-S. *Appl. Catal., A* **2015**, *492*, 252–261.
- Ordonsky, V. V.; Sushkevich, V. L.; Schouten, J. C.; van der Schaaf, J.; Nijhuis, T. A. *J. Catal.* **2013**, *300*, 37–46.
- Siankevich, S.; Savoglidis, G.; Fei, Z.; Laurenczy, G.; Alexander, D. T. L.; Yan, N.; Dyson, P. J. *J. Catal.* **2014**, *315*, 67–74.
- Albonetti, S.; Lolli, A.; Morandi, V.; Migliori, A.; Lucarelli, C.; Cavani, F. *Appl. Catal., B* **2015**, *163*, 520–530.
- Kirilina, A.; Wärnå, J.; Tokarev, A.; Murzin, D. Y. *Ind. Eng. Chem. Res.* **2014**, *53*, 4580–4588.
- van Haasterecht, T.; Ludding, C. C. I.; de Jong, K. P.; Bitter, J. H. *J. Catal.* **2014**, *319*, 27–35.
- Liu, D.; Chen, E. Y.-X. *ACS Catal.* **2014**, *4*, 1302–1310.
- Miranda, B. C.; Chimentão, R. J.; Santos, J. B. O.; Gispert-Guirado, F.; Llorca, J.; Medina, F.; Bonillo, F. L.; Sueiras, J. E. *Appl. Catal., B* **2014**, *147*, 464–480.
- Lautenschläger, C. L.; Bockmühl, M.; Ehrhart, G.; Kroß, W. German Patent 541,362, 1932.
- Lautenschläger, K. L.; Bockmühl, M.; Ehrhart, G.; Krohs, W. U.S. Patent 1,915,431, 1933.
- Larcher, A. W. (to Du Pont Co.) U.S. Patent 1,963,997, 1934.
- Rothrock, H. S. (to Du Pont Co.), U.S. Patent 2,004,135, 1935.
- Ruppert, A. M.; Weinberg, K.; Palkovits, R. *Angew. Chem., Int. Ed.* **2012**, *51*, 2564–2601.
- Chopade, S. P.; Miller, D. J.; Jackson, J. E.; Werpy, T. A.; Frye, J. G., Jr.; Zacher, A. H. U.S. Patent 6,291,725 B1, 2001.
- Werpy, T. A.; Frye, J. G., Jr.; Zacher, A. H.; Miller, D. J. U.S. Patent 6,677,385 B2, 2004.
- Werpy, T. A.; Frye, J. G., Jr.; Zacher, A. H.; Miller, D. J. U.S. Patent 6,841,085 B2, 2005.
- Liu, Y.; Luo, C.; Liu, H. *Angew. Chem., Int. Ed.* **2012**, *51*, 3249–3253.
- Yepez, A.; Pineda, A.; Garcia, A.; Romero, A. A.; Luque, R. *Phys. Chem. Chem. Phys.* **2013**, *15*, 12165–12172.
- Ooms, R.; Dusselier, M.; Geboers, J. A.; Op de Beeck, B.; Verhaeven, R.; Gobechiya, E.; Martens, J. A.; Redl, A.; Sels, B. F. *Green Chem.* **2014**, *16*, 695–707.
- Song, J.; Fan, H.; Ma, J.; Han, B. *Green Chem.* **2013**, *15*, 2619–2635.
- Kobayashi, H.; Fukuoka, A. *Green Chem.* **2013**, *15*, 1740–1763.
- Miao, G.; Zhu, C. C.; Wang, J. J.; Tan, Z. C.; Wang, L.; Liu, J. L.; Kong, L. Z.; Sun, Y. H. *Green Chem.* **2015**, *17*, 2538–2544.

- (31) Wang, X.; Meng, L.; Wu, F.; Jiang, Y.; Wang, L.; Mu, X. *Green Chem.* **2012**, *14*, 758–765.
- (32) Zhang, J.; Hou, B.; Wang, A.; Li, Z.; Wang, H.; Zhang, T. *AIChE J.* **2014**, *60*, 3804–3813.
- (33) Wang, K.; Hawley, M. C.; Furney, T. D. *Ind. Eng. Chem. Res.* **1995**, *34*, 3766–3770.
- (34) Zhao, G.; Zheng, M.; Zhang, J.; Wang, A.; Zhang, T. *Ind. Eng. Chem. Res.* **2013**, *52*, 9566–9572.
- (35) Zheng, M.; Wang, A.; Ji, N.; Pang, J.; Wang, X.; Zhang, T. *ChemSusChem* **2010**, *3*, 63–66.
- (36) Tai, Z.; Zhang, J.; Wang, A.; Zheng, M.; Zhang, T. *Chem. Commun.* **2012**, *48*, 7052–7054.
- (37) Sifontes Herrera, V. A.; Oladele, O.; Kordás, K.; Eränen, K.; Mikkola, J.-P.; Murzin, D. Yu.; Salmi, T. *J. Chem. Technol. Biotechnol.* **2011**, *86*, 658–668.
- (38) Li, N.; Huber, G. W. *J. Catal.* **2010**, *270*, 48–59.
- (39) You, S. J.; Baek, I. G.; Park, E. D. *Appl. Catal., A* **2013**, *466*, 161–168.
- (40) Holm, M.; Saravanamurugan, S.; Taarning, E. *Science* **2010**, *328*, 602–605.
- (41) Sasaki, M.; Goto, K.; Tajima, K.; Adschiri, T.; Arai, K. *Green Chem.* **2002**, *4*, 285–287.
- (42) Kanie, Y.; Akiyama, K.; Iwamoto, M. *Catal. Today* **2011**, *178*, 58–63.
- (43) Vispute, T. P.; Huber, G. W. *Green Chem.* **2009**, *11*, 1433–1445.
- (44) Zhao, C.; Kou, Y.; Lemonidou, A. A.; Li, X.; Lercher, J. A. *Angew. Chem., Int. Ed.* **2009**, *48*, 3987–3990.
- (45) Hong, Y. K.; Lee, D. W.; Eom, H. J.; Lee, K. Y. *Appl. Catal., B* **2014**, *150–151*, 438–445.
- (46) Román-Leshkov, Y.; Davis, M. E. *ACS Catal.* **2011**, *1*, 1566–1580.
- (47) Ekeberg, D.; Morgenlie, S.; Stenström, Y. *Carbohydr. Res.* **2005**, *340*, 373–377.
- (48) Ross-Medgaarden, E. I.; Wachs, I. E. *J. Phys. Chem. C* **2007**, *111*, 15089–15099.
- (49) Kim, T.; Burrows, A.; Kiely, C. J.; Wachs, I. E. *J. Catal.* **2007**, *246*, 370–381.
- (50) Chen, X.; Clet, G.; Thomas, K.; Houalla, M. *J. Catal.* **2010**, *273*, 236–244.
- (51) Wu, X.; Zhang, L.; Weng, D.; Liu, S.; Si, Z.; Fan, J. *J. Hazard. Mater.* **2012**, *225–226*, 146–154.
- (52) Ghosh, S.; Acharyya, S. S.; Tiwari, R.; Sarkar, B.; Singha, R. K.; Pendem, C.; Sasaki, T.; Bal, R. *ACS Catal.* **2014**, *4*, 2169–2174.
- (53) Fu, L.; Xia, T.; Zheng, Y.; Yang, J.; Wang, A.; Wang, Z. *Ceram. Int.* **2015**, *41*, 5903–5908.
- (54) Mamede, A.-S.; Leclercq, G.; Payen, E.; Granger, P.; Grimblot, J. *J. Mol. Struct.* **2003**, *651–653*, 353–364.
- (55) Moraes, R.; Thomas, K.; Thomas, S.; Van Donk, S. V.; Grasso, G.; Gilson, J.-P.; Houalla, M. *J. Catal.* **2012**, *286*, 62–77.
- (56) Taylor, M. N.; Zhou, W.; Garcia, T.; Solsona, B.; Carley, A. F.; Kiely, C. J.; Taylor, S. H. *J. Catal.* **2012**, *285*, 103–114.
- (57) Contreras, J. L.; Fuentes, G. A.; García, L. A.; Salmones, J.; Zeifert, B. *J. Alloys Compd.* **2009**, *483*, 450–452.
- (58) García-Fernández, S.; Gandarias, I.; Requies, J.; Güemez, M. B.; Bennici, S.; Auroux, A.; Arias, P. L. *J. Catal.* **2015**, *323*, 65–75.
- (59) Karim, A. H.; Triwahyono, S.; Jalil, A. A.; Hattori, H. *Appl. Catal., A* **2012**, *433–434*, 49–57.
- (60) Onfroy, T.; Clet, G.; Houalla, M. *J. Phys. Chem. B* **2005**, *109*, 3345–3354.
- (61) Baertsch, C. D.; Soled, S. L.; Iglesia, E. *J. Phys. Chem. B* **2001**, *105*, 1320–1330.
- (62) Kim, T. Y.; Park, D. S.; Choi, Y.; Baek, J.; Park, J. R.; Yi, J. *J. Mater. Chem.* **2012**, *22*, 10021–10028.
- (63) Sun, D.; Yamada, Y.; Sato, S. *Appl. Catal., A* **2014**, *487*, 234–241.
- (64) Ooms, R.; Dusselier, M.; Geboers, J. A.; Op de Beeck, B.; Verhaeven, R.; Gobechiya, E.; Martens, J. A.; Redl, A.; Sels, B. F. *Green Chem.* **2014**, *16*, 695–707.
- (65) Watanabe, M.; Aizawa, Y.; Iida, T.; Nishimura, R.; Inomata, H. *Appl. Catal., A* **2005**, *295*, 150–156.
- (66) Román-Leshkov, Y.; Moliner, M.; Labinger, J. A.; Davis, M. E. *Angew. Chem., Int. Ed.* **2010**, *49*, 8954–8957.
- (67) Choudhary, V.; Mushrif, S. H.; Ho, C.; Anderko, A.; Nikolakis, V.; Marinkovic, N. S.; Frenkel, A. I.; Sandler, S. I.; Vlachos, D. G. *J. Am. Chem. Soc.* **2013**, *135*, 3997–4006.
- (68) Liu, N.; Ding, S.; Cui, Y.; Xue, N.; Peng, L.; Guo, X.; Ding, W. *Chem. Eng. Res. Des.* **2013**, *91*, 573–580.
- (69) Samain, L.; Jaworski, A.; Edén, M.; Ladd, D. M.; Seo, D.-K.; Javier Garcia-Garcia, F.; Häussermann, U. *J. Solid State Chem.* **2014**, *217*, 1–8.
- (70) Dou, X.; Mohan, D.; Zhao, X.; Pittman, C. U., Jr. *Chem. Eng. J.* **2015**, *264*, 617–624.